Effect of Inclined Transverse Jets on Trailing-Edge Noise Generation

Máté Szőke,[1, a)] Daniele Fiscaletti,[1] and Mahdi Azarpeyvand[1]

Faculty of Engineering, University of Bristol, Bristol, England BS8 1TR, United Kingdom

(Dated: 4 September 2018)

In this work, the effect of multiple transverse jets on the turbulent boundary layer developing over a flat plate is experimentally investigated for aeroacoustic purposes. A single line of jet nozzles with different spanwise spacings is located parallel to the trailing-edge of the plate, at approximately 30 jet diametres upstream of the trailing-edge. The axes of the jet nozzles have an inclination of 15 degrees with respect to the streamwise direction. Two values of the jet velocity ratio ($r = u_{jet}/u_\infty$) are considered, $r = 1$ and $r = 2$. The simultaneous measurement of streamwise velocity and surface pressure fluctuations is performed with hot-wire anemometry and flush-mounted microphones, respectively. The mean velocity profiles show that the low inclination angle of the multiple jets prevents the formation of adverse pressure gradients, and therefore the multiple jets injection does not lead to flow separation, at least at the range of downstream locations under investigation. From the velocity measurements, the jets merge downstream of the jet nozzles, and form a layer of jet fluid characterized by a low energy content. The estimates of the far-field noise show that jets injection at a velocity ratio of $r = 1$ leads to noise attenuation over the whole range of frequencies under analysis. At a velocity ratio of $r = 2$, jets injection enables to gain a larger noise reduction than at $r = 1$ at low frequencies, but the estimated far-field noise is expected to increase at high frequencies.

[a)]Electronic mail: m.szoke@bristol.ac.uk; Faculty of Engineering, University of Bristol, Bristol, England BS8 1TR, United Kingdom

I. INTRODUCTION

In the last decades, researches have shown that the sound generated by the turbulence around an airfoil represents one of the dominant sources of noise from airplanes, turbomachines, and wind farms[1,2]. According to Brooks *et al.*[2], the broadband trailing-edge noise emitted by an airfoil in movement inside a fluid is the dominant component of airfoil noise. The reduction of trailing-edge noise therefore represents an important engineering challenge. With the aim of mitigating the trailing-edge noise, several studies were conducted since the 1970s[1,3–7], when the first legislations limiting noise pollution began to be issued[8]. These pioneering studies could shed light on the mechanism for the trailing-edge noise generation. In particular, it was shown that as the hydrodynamic pressure field associated with the turbulent boundary layer passes over the trailing-edge, the pressure field scatters into sound in a dipole manner. As a result, there are two possible strategies to reduce the trailing-edge noise, which are (i) changing the manner the pressure field scatters into sound, and (ii) controlling the pressure field within the boundary layer upstream of the trailing-edge.

Based on this observation, a number of different trailing-edge noise reduction methods were proposed over the past few decades. The majority of these studies applied *passive methods*, where physical and geometrical properties of the trailing-edge were altered, such that it favourably affected the noise scattering mechanism. Examples of passive methods are the trailing-edge serrations[9–11], trailing-edge brushes[12], porous material[13,14], surface treatments[15,16], shape optimization, and morphing[17,18], etc. Passive methods are limited to a given range of conditions, and outside of this range they might induce undesired losses in the aerodynamic performance. Additionally, should the noise reduction requirements change during machine operation, passive methods can not be adjusted. *Active methods* target the alteration of the hydrodynamic pressure field within the turbulent boundary layer upstream of the trailing-edge. It is worth highlighting that according to the present definition of *active flow control methods* both open-loop and close-loop flow control methods considered. Despite the *active methods* have received a limited attention from the aeroacoustics community[19–22], they offer a number of positive aspects. Their advantages are that they can be adjusted to meet the actual noise reduction needs, they could produce higher levels of noise attenuation than *passive methods*, and they can lead to an improvement of the aerodynamic performance. However, their main drawback is that they require a supply of external energy. An effec-

tive *active flow control method* must reduce the hydrodynamic pressure fluctuations at the price of a low energy intake, while not altering the aerodynamic performance of the airfoil. Suction from or injection into the boundary layer can be considered as the two fundamental *active methods*.

Flow suction is effective in reducing the surface pressure field, but, as can be inferred from the works of Wolf *et al.*[19] and Szőke *et al.*[23], this method requires a large energy supply, and it has significant maintenance costs. On the other hand, flow injection[21–24] requires a lower amount of external energy than flow suction. With the aim of minimizing the demand of external power supply, inclined transverse jets can be used in place of uniform blowing. Szőke *et al.*[23] recently conducted preliminary studies on the use of inclined uniform injection as an *active flow control method*. In their experimental investigations[23], the authors reported that reducing the blowing angle of the uniform flow injection could lower the absorption of external energy, and, at the same time, could prevent flow detachment, which could occur when applying steady blowing. It was observed that inclined transverse jets could result in a reduction of the surface pressure fluctuations, thus exhibiting potentials for aeroacoustics applications. Nonetheless, the previous works focusing on the use of active flow control methods to mitigate the trailing-edge noise[19,21,22] do not clarify how the main parameters of the flow control methods affect the turbulence of the boundary layer and the associated surface pressure field. A deeper understanding of the flow structure generated when jets interact with a boundary layer is therefore necessary, with the aim of conveniently setting the flow control parameters.

The problem of a jet in a crossflow has received a significant attention in the past few years[25,26]. Although the geometry of the problem is simple, this flow can result in a range of different complex flow structures, which were observed to change with the jet nozzle velocity, the crossflow velocity, and the jet inclination angle. In particular, two main non-dimensional parameters were observed to govern the problem, i.e. the jet velocity ratio, r, which is the ratio of jet velocity (u_{jet}) to the crossflow velocity (u_∞), and $J = \varrho_{jet} u_{jet}^2 / \varrho_\infty u_\infty^2$, the momentum flux ratio. In several engineering applications, jet flows can be observed to interact with a crossflow developing over a plate. Examples of this are the use of jets for cooling the blades of a gas-turbine engine, or to control the levels of nitrogen oxide produced in the combustion chamber of an internal engine, or to enhance turbulent mixing. From a detailed analysis of the literature on this problem, several experimental and numerical studies

were performed to mimic the engineering problem of the turbine blade cooling, with the aim of enhancing the cooling performance[27–30]. In particular, low velocity ratios ($r < 2$) were considered for boundary layers at a laminar regime, or at a low Reynolds number. The jets were observed to form a stable fluid film over the surface to cool, and to isolate the high temperature mean flow from the blades. The jet incidence angle was also investigated[31–33]. It was found that, if the jet inclination angle is below 30°, the boundary layer flow remains attached to the wall. Significant differences exist between the application of transverse jets to enhance the cooling of a turbine blade and to mitigate the trailing-edge noise. In aeroacoustics, the crossflow is characterized by higher turbulence levels and larger ratios of boundary layer thickness over jet diameter. These differences make the characterisation of the flow observed in the turbine blade cooling not particularly relevant to the problem of trailing-edge noise mitigation.

Despite it was developed a few decades ago, Amiet's model for the prediction of trailing-edge noise[7] is still rather popular within the aeroacoustic community. This model states that the far-field trailing-edge noise is directly proportional to two quantities involving the surface pressure fluctuations at the trailing-edge. These quantities are the power spectrum at the centerline of the trailing-edge and the integral of the spanwise coherence along the trailing-edge. Nonetheless, the effect of transverse jets on the surface pressure fluctuations has scarcely been explored[34]. Therefore, despite the surface pressure fluctuations enter in the model for the prediction of trailing-edge noise[7], their sensitivity to the transverse jets is still unknown. In the present work, we aim at investigating experimentally the hydrodynamic effects of inclined transverse jets on the boundary layer over a flat plate of finite length, for aeroacoustic purposes. Hot-wire anemometry and flush mounted microphones are used to measure the velocity and pressure fluctuations associated with the boundary layer.

The current paper is organised as follows. Section II describes the measurement conditions, the experimental set-up, the geometrical properties relevant to the experimental investigation, and introduces Amiet's trailing-edge noise model, which establishes the link between the flow properties and the emitted far-field noise. Section III provides the characterisation of the flow structure, as obtained from hot-wire anemometry and microphone measurements. Once the hydrodynamic flow structure is understood, its effects on the trailing-edge noise generation is evaluated by investigating the interaction between pressure and velocity fluctuations.

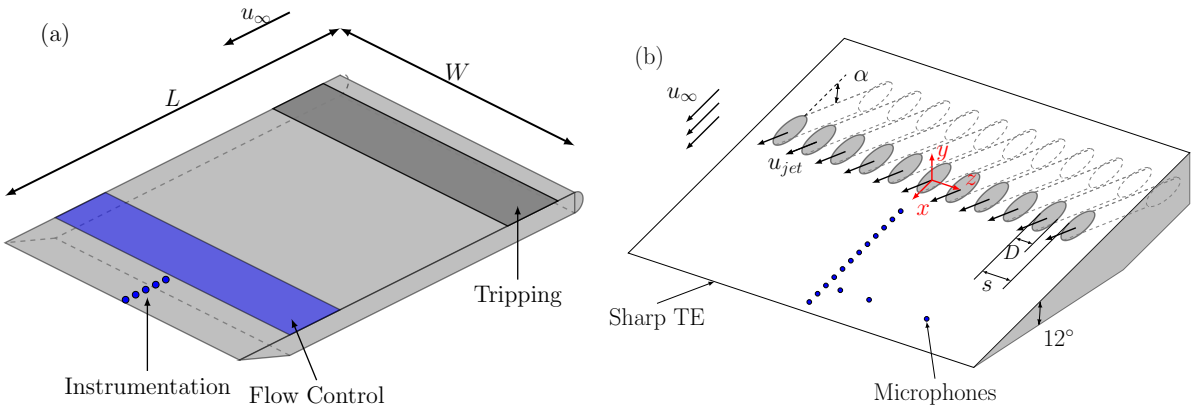

FIG. 1. Schematic of the rig (a) and the trailing-edge (b).

II. EXPERIMENTAL APPROACH

A. Test Rig Set-up and Instrumentation

Experiments have been conducted in the open-jet return-type wind tunnel facility of the University of Bristol. A zero pressure gradient flat plate with a length of $L = 1$ m and a width of $W = 0.7$ m was built, which ends in a sharp (12°) trailing-edge, see Fig. 1. An 80 grit sandpaper was mounted immediately after the plate semi-elliptical leading edge to trigger the development of the turbulent boundary layer on the surface of the plate. Tests were carried out at a uniform flow velocity of $u_\infty = 15$ m/s, corresponding to a Reynolds number of $Re_L = 10^6$ based on the length of the plate ($Re_L = u_\infty L/\nu$).

Flush mounted electret condenser microphones were used for the measurement of the surface pressure fluctuations. A total number of 21 pressure transducers were positioned along the streamwise and the spanwise directions, and in the vicinity of the trailing-edge (see Fig. 1). The miniature FG-23329-P07 type Knowles microphones were calibrated prior to the measurements. Their sensitivity leads to a measurement accuracy of ±0.5 dB within the frequency range of interest ($10^2 - 10^4$ Hz). The uncertainty of the microphones was determined based on the method of Kline and McClintock[35]. Schewe[36] reported that when the dimensionless sensing diameter of the microphones ($d^+ = du_\tau/\nu$) exceeds $d^+ = 19$, the attenuation of the pressure signal can be corrected using the correction method proposed by Corcos[37], based on transducer resolution. In this experimental campaign, the dimensionless sensing diameter is $d^+ = 35$, therefore the pressure attenuation introduced by the finite

extent of the microphone diaphragm was corrected using Corcos' method[37]. Additionally, the microphones were mounted below a small pinhole with a diameter of $d_p = 0.4$ mm, which corresponds to a dimensionless pinhole diameter of $d_p^+ = d_p u_\tau/\nu = 19$. The preliminary hot-wire measurements confirmed that the surface discontinuity introduced by the pinholes does not affect the boundary layer.

The streamwise component of the velocity was measured with hot-wire anemometry, to characterise the boundary layer flow downstream of the jet nozzles. Dantec 55P16 type single-sensor hot-wire probes were operated by a Dantec StreamWare Pro CTA91C10 module, at an overheat ratio of 1.8. The diameter and the length of the hot-wire sensor used here are 5 μm and 1.25 mm, which are equivalent to 0.2 and 53 viscous units, respectively. The measurement probe was calibrated prior to the measurements on a daily basis, and its uncertainty was found to be less than 0.5 % over the whole range of velocities under investigation. Data were collected by a National Instruments PXIe-4499 system, at a sampling rate of $f_s = 65{,}536$ Hz ($=2^{16}$ Hz), for a time span of 16 seconds, at each measurement location. Data processing was performed with the use of Python's SciPy package. For the calculation of both spectra and coherence, a digital filter was applied in order to reduce the effects of low frequency background noise[38]. Time signals were divided into smaller segments with a 50 % overlapping. The length of these segments (i.e. window size, WS) was defined such that the frequency resolution of the signal was $\Delta f = 64$ Hz, with $\Delta f = 4f_s/WS$. Hamming windowing was then applied to all the segments, which was followed by the calculation of their fast Fourier transform. After the Fourier transform of each segment, the energy loss in the signal resulting from the application of Hamming windowing was compensated a posteriori, and the obtained spectra were averaged.

B. Active Flow Control Parameters

Along the spanwise direction, a single array of inclined jets has been placed on the flat plate as boundary layer flow manipulation method, with the aim of reducing the trailing-edge noise. Figure 1 gives the geometrical description of the active flow control method and provides the definition of the coordinate system. The coordinate system consists of the streamwise (x), the wall normal (y), and the spanwise (z) directions, and its origin is located at the centre of the jet nozzle at the half-span of the plate. The jet nozzles are

circular in shape, with a diameter of $D = 4$ mm, and inclined by $\alpha = 15^\circ$ with respect to the x axis. The length-to-diameter ratio of the jet nozzles is $l_j/D = 5$. The nozzles are located $30D$ upstream of the trailing-edge to ensure that the jets can fully develop before reaching the trailing-edge. Air to the jet nozzles was supplied using an industrial fan. The compressed air was fed into a settling chamber mounted underneath the plate, after which it was discharged through the jets. The settling chamber had also the effect of producing a steady-state flow through the jet nozzles. An inverter enabled the accurate control of the fan power, which was used to adjust the jet velocity. It is worth stressing that the proposed flow control method is based on an open-loop control. The background noise associated with the simultaneous operation of the open-jet wind tunnel facility and the industrial fan has been measured during preliminary tests. The boundary layer pressure results will be provided only when the measured pressure is at least 10 dB higher than the background noise. The jet spacing (s), i.e. the spanwise distance between the jet nozzles, is defined in terms of jet diameter D (see Fig. 1), and six spacings are considered in this study, namely $1.5D$, $2.0D$, $2.5D$, $3.0D$, $3.5D$ and $4.0D$.

The flow control severity, σ, relates the momentum deficit of the boundary layer to the momentum of the flow control system. According to Antonia *et al.*[39], the level of flow control can be quantified as follows:

$$\sigma = \frac{u_{jet} D \varphi}{u_\infty \theta_0}, \tag{1}$$

where u_{jet} is the mean velocity of the jets in the nozzles, D is the jet nozzle diameter, $u_\infty = 15$ m/s is the free-stream flow velocity, φ is the porosity parameter, finally, θ_0 is the momentum thickness of the non-disturbed boundary layer.

The porosity parameter (φ) relates the total area occupied by the jets (nA_{jet}) to the overall flow control section area (bD, with b being the width of the flow control section), and can be written in the form of $\varphi = A_{jet}/(sD)$. The porosity is defined in the plane perpendicular to the axes of the jet nozzle (see Fig. 2). Substituting this expression of φ in Eq. (1) results in $\sigma = rA_{jet}/(\theta_0 s)$, where $r = u_{jet}/u_\infty$ is the jet velocity ratio. A range of jet velocity ratios $0 \leq r \leq 2$ is considered in this study but more detailed results and discussions will be provided for $r = 0$ (baseline case), $r = 1$ and $r = 2$. The flow control settings considered in the current study and the corresponding boundary layer parameters are listed in Table II.

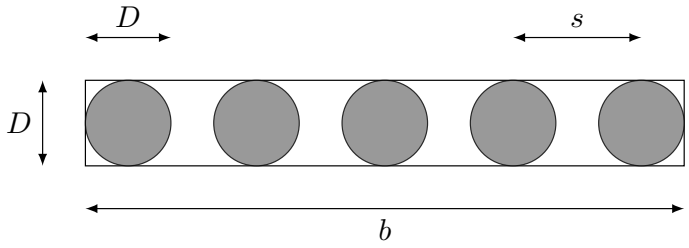

FIG. 2. The definition of the jet nozzle porosity.

C. Amiet's Trailing-Edge Noise Model

The proper measurement of the far-field trailing-edge noise requires the use of an anechoic wind tunnel. Nonetheless, several physical models were developed in the last few decades[2,7,40], which establish a relationship between surface pressure fluctuations and turbulence within the flow on one side, and far-field noise on the other side. Therefore, pressure and velocity measurements from conventional wind tunnels can be used as input parameters for the aforementioned models of far-field trailing-edge noise. In the current work, Amiet's model[7], presented in the following, is used.

According to Amiet's trailing-edge model, the far-field noise (S_{pp}) at a far-field distance from the trailing-edge centre line of the flat plate ($x, y, z = 0$), can be found from

$$S_{pp}(x, y, z = 0, f) = \left(\frac{fLy}{4\pi c_0 \xi^2}\right)^2 \frac{W}{2} |\mathcal{L}|^2 \Lambda_z(f) \phi_{pp}(f), \tag{2}$$

where f denotes frequency, c_0 is the speed of sound, $\xi^2 = x^2 + (1 - u_\infty/c_0)^2 y^2$ is the convection-corrected far-field observer position, L is the length of the plate (chord), W is the width of the plate, $\mathcal{L}$ is the gust response transfer function[41], Λ_z and ϕ_{pp} are, respectively, the spanwise extent of the turbulent structures within the boundary layer, and the power spectrum of the surface pressure fluctuations near the trailing-edge. Amiet's model works under the assumption of stationary turbulence. A more detailed description and the derivation of the model is given by Amiet[5,7]. According to Amiet's model, the product $\Lambda_z \phi_{pp}$ drives the generated far-field noise, therefore the reduction of this product determines the success of a noise attenuation method. The surface pressure power spectrum (ϕ_{pp}) is directly measured in the current work, while the spanwise extent of the turbulent structures (Λ_z) can be calculated from surface pressure fluctuations as follows[7]:

$$\Lambda_z(f) = \int_0^\infty \sqrt{\gamma_z^2(f, \zeta)} \mathrm{d}\zeta, \tag{3}$$

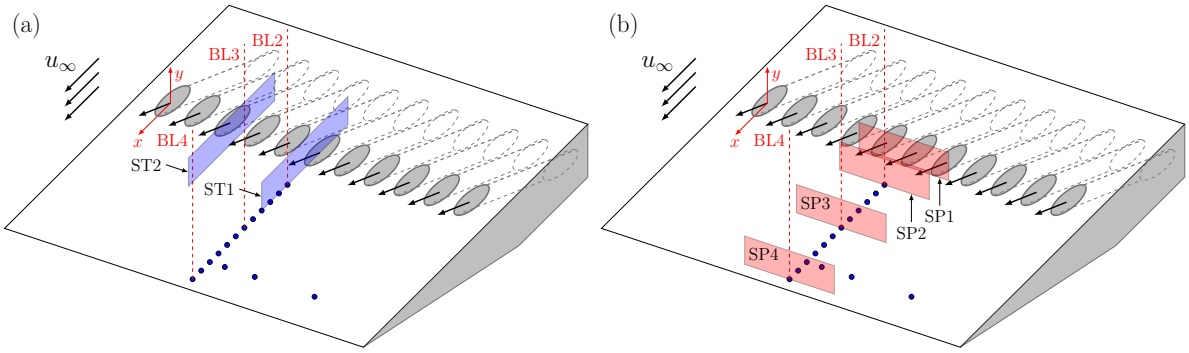

FIG. 3. Schematics of the streamwise (ST), spanwise (SP) and boundary layer (BL) hot-wire measurements.

	ST1	ST2	SP1	SP2	SP3	SP4	BL2	BL3	BL4
x/D	[-3, 10]	[-3, 10]	2	4	14	30	4	14	30
y/δ_0	[0, 0.2]	[0, 0.2]	[0, 0.2]	[0, 0.2]	[0, 0.2]	[0, 0.2]	[0, 1]	[0, 1]	[0, 1]
z/D	0	1.25	[-4, 4]	[-4, 4]	[-4, 4]	[-4, 4]	0	0	0

TABLE I. The areas covered by traversing the hot-wire sensor in the different sets of measurements.

where $\gamma_z^2(f,\zeta)$ represents the spanwise cross-spectrum of surface pressure fluctuations acquired from two microphones located in the proximity to the trailing-edge, with a spanwise separation distance of $\zeta = \Delta z$. The cross-spectrum (coherence) can be interpreted as the the spanwise extent of turbulent structures. In the current work, the spanwise coherence is measured at a streamwise distance of $3D$ upstream of the trailing-edge (see Fig. 1). The thickness of the plate at this location is larger than the height of the pressure transducers, therefore they do not introduce disturbances to the flow underneath of the rig.

III. RESULTS AND DISCUSSIONS

The results obtained from the hot-wire and microphone measurements are presented and discussed in the present section. Figure 3 illustrates the three sets of measurements considered in the current study. Firstly, the streamwise velocity was measured with hot-wire anemometry along the whole wall-normal span of the turbulent boundary layer thickness, at three different streamwise locations, marked as BL2, BL3 and BL4 (see the red dashed lines

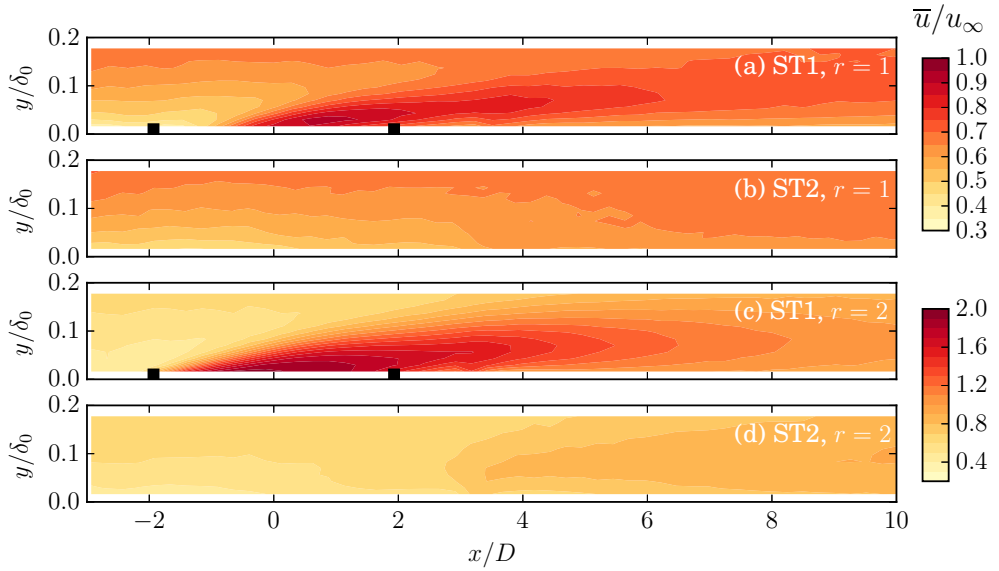

FIG. 4. Mean velocity as obtained from the hot-wire anemometry, along the streamwise plane sections ST1 and ST2 for the velocity ratios $r = 1$ and $r = 2$ and for nozzle spacing $s = 2.5D$ (■ denotes the upstream and downstream edges of the jet nozzles).

in Fig. 3). Signals from the hot-wire sensor and the microphone located at the corresponding x location were recorded simultaneously. Secondly, the hot-wire sensor was traversed along the $x-y$ and $y-z$ planes. This set of measurements enabled to observe the effect of the jets in the wall-normal direction, at different streamwise and spanwise cross sections. The velocity was measured over two streamwise planes, ST1 and ST2, located at the center of a jet, and half-way between two neighbouring jets, respectively (see Fig. 3). The $y-z$ measurement planes are labelled in Fig. 3 with SP1, SP2, SP3 and SP4. The locations covered by the hot-wire anemometry measurements are listed in Table I. All planar measurements were restricted to the lower fifth of the wall-normal extent of the boundary layer, therefore in the region $[0,0.2\delta_0]$. In the third set of measurements, the signals from all flush mounted microphones were simultaneously recorded. This last set of measurements enabled us to calculate the spanwise coherence and the power spectral density of the surface pressure fluctuations.

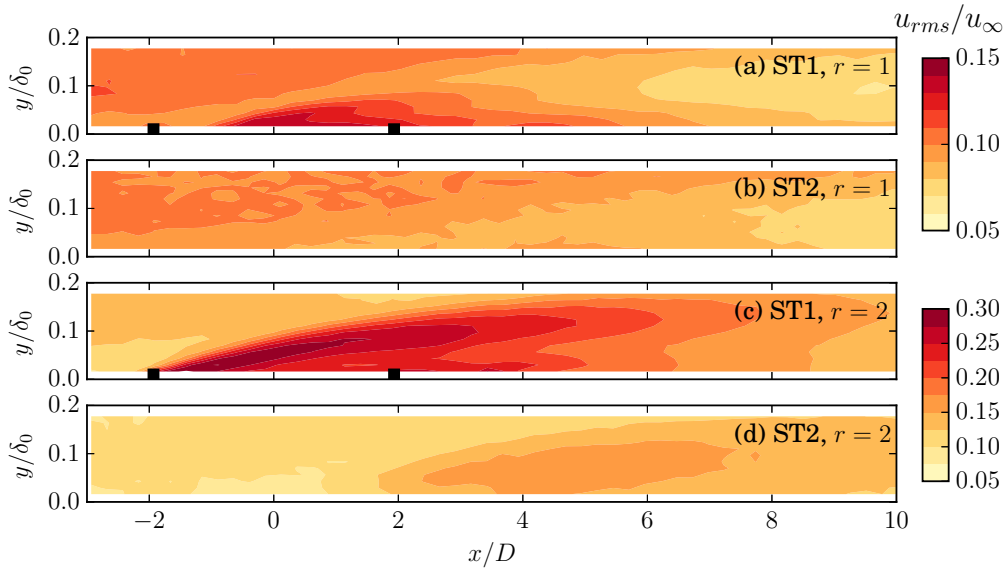

FIG. 5. Root mean square (rms) velocity as obtained from the hot-wire anemometry, along the streamwise plane sections ST1 and ST2 for the velocity ratios $r = 1$ and $r = 2$ and for nozzle spacing $s = 2.5D$ (■ denotes the upstream and downstream edges of the jet nozzles).

A. The Developing Flow Pattern

Based on the described sets of measurements, the developing flow pattern produced by the injection of multiple jets is examined, including its effects on the surface pressure fluctuations. Turbulence statistics, such as the mean velocity ($\bar{u}$) and root mean square velocity (i.e. energy content, u_{rms}) enable us to assess the main properties of the flow. The mean and root mean square (rms) velocity results reveal the effects of the jets on the boundary layer flow. The properties of the baseline boundary layer ($r = 0$) are presented after discussing the hot-wire measurements along the planes ST and SP. In the following, the analysis of the flow is limited to the jet spacing of $s = 2.5D$, while the effect of jet spacing will be examined in Section III B. Figures 4 and 5 provide the contour plots of the mean ($\bar{u}$) and the root mean square (u_{rms}) velocities obtained in the planes ST1 and ST2, for both the considered velocity ratios, i.e. $r = 1$ and $r = 2$. The streamwise direction was non-dimensionalized by the jet nozzle diameter (D), while the wall-normal direction by the baseline ($r = 0$) boundary layer thickness (δ_0). The black squares on the x-axis mark the edges of the jet nozzle on the plane ST1. The hot-wire probe was traversed over the ST1 and ST2 planes

with streamwise and wall-normal spacings of $\Delta x/D = 0.25$ and $\Delta y/\delta_0 = 0.015$, respectively.

The results reveal that the potential core of the jets remains in the vicinity of the wall, indicating that the jets develop in the near-wall region regardless of the applied velocity ratio. The proximity of the jets with respect to the wall confirms that the jets do not trigger boundary layer separation, which is in agreement with the results of Taylor[31,32], who found that when the jet inclination angle is kept below $\alpha = 30^\circ$ the boundary layer flow remains attached to the wall. The root mean square velocity distributions along ST1 in Fig. 5 show that the upper and the lower edges of the jets are characterised by a high energy flow content. These larger values of u_{rms} were also reported by former studies[34,42,43], where these regions of large u_{rms} were found to be associated with the presence of intense shear. The energy content found in the upper edge of the jet is higher than the energy content obtained in the lower edge, which is consistent with the results of Pietrzyk *et al.*[44]. The energy content of the flow structures associated with the interaction of the jet flow with the boundary layer flow decays fast with x/D, with a rate higher than that of the boundary layer. This decay in the energy content is significant, as it even leads to a drop below the value obtained upstream of the jet nozzles. This observation is confirmed by comparing the u_{rms} values for the $r = 1$ case, at ST1 and ST2 (see Fig. 5), upstream and downstream of the jet nozzles. For $r = 2$, a similar trend is observed, as an initial increase of u_{rms} is visible, followed by a drop. However, this decrease does not lead to u_{rms} reaching the baseline value, even at $x/D = 10$. This suggests that by increasing the velocity ratio, the flow turbulence requires a longer streamwise distance to obtain a reduction in its energy content. The lower energy content observed in proximity to the wall results in lower amplitudes of the surface pressure fluctuations, which can subsequently lead to the reduction of trailing-edge noise. This is going to be further investigated in Section III B, following the current discussion on the turbulence statistics.

The spanwise flow patterns obtained downstream of the jet nozzles can be investigated by calculating the turbulence statistics along the spanwise planes, at different streamwise locations. Figures 6 and 7 provide the contour plots of the mean ($\bar{u}$) and the root mean square (u_{rms}) streamwise velocities obtained for both velocity ratios ($r = 1$ and $r = 2$), over the SP1, SP2, SP3 and SP4 planes, located at the downstream locations of $x/D = 2, 4, 14$ and 30, respectively, with respect to the centre of the jet nozzles. The hot-wire probe was traversed over the planes identified with SP in Figs. 6 and 7 with a wall-normal and spanwise

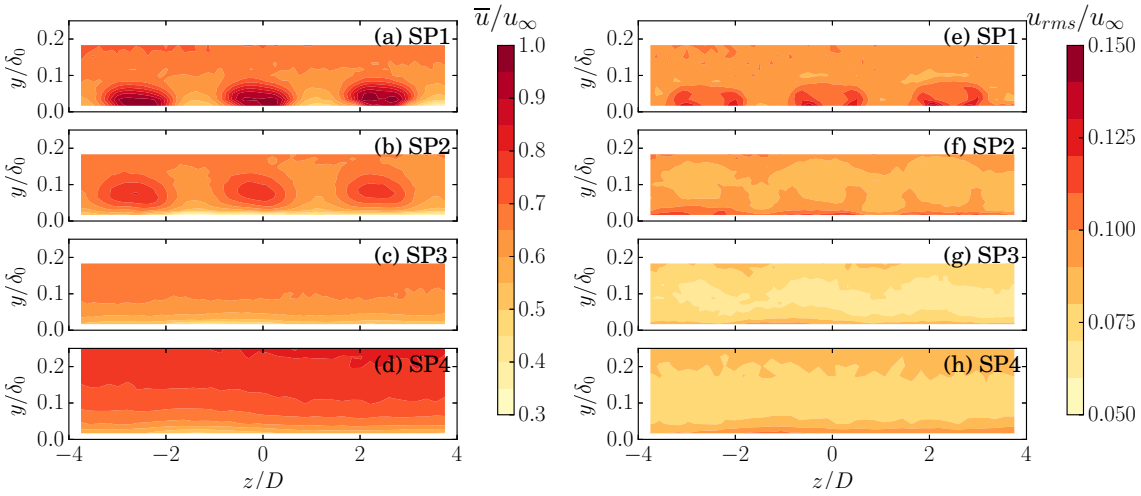

FIG. 6. Mean and root mean square (*rms*) velocity as obtained from the hot-wire anemometry along the spanwise plane sections SP1, SP2, SP3 and SP4 for the velocity ratio $r = 1$ and for nozzle spacing $s = 2.5D$.

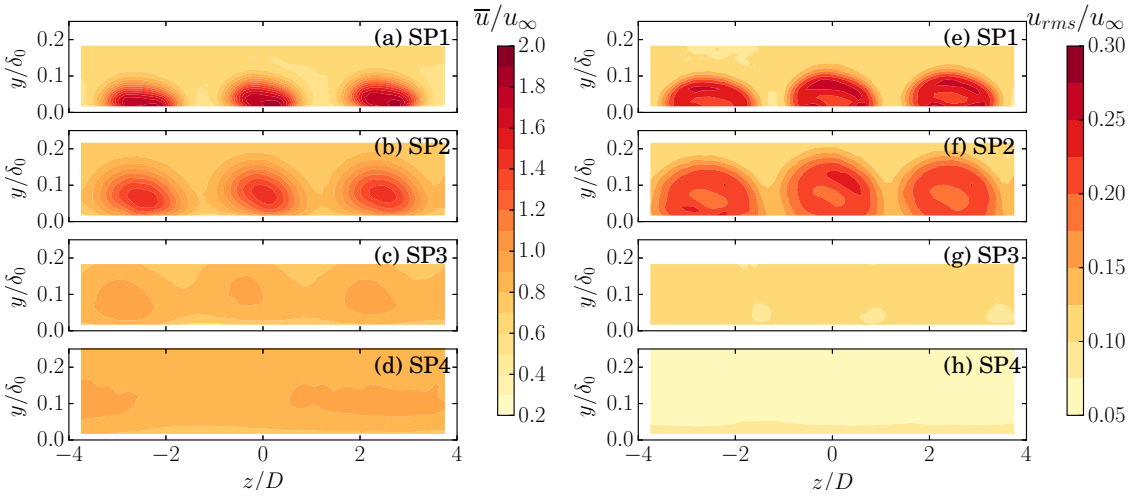

FIG. 7. Mean and root mean square (*rms*) velocity as obtained from the hot-wire anemometry along the spanwise plane sections SP1, SP2, SP3 and SP4 for the velocity ratio $r = 2$ and for nozzle spacing $s = 2.5D$.

spacings of $\Delta y/\delta_0 = 0.015$ and $\Delta z/D = 0.125$, respectively. In agreement with previous studies[45], the flow patterns resulting from the jet array are not circular in shape at ST1 and ST2, but elongated along the spanwise direction. The footprints of the jets are well separated in each contour plots at SP1 and SP2 for both velocity ratios, which suggests that they are distinguishable at these two streamwise locations. The observed jet footprints

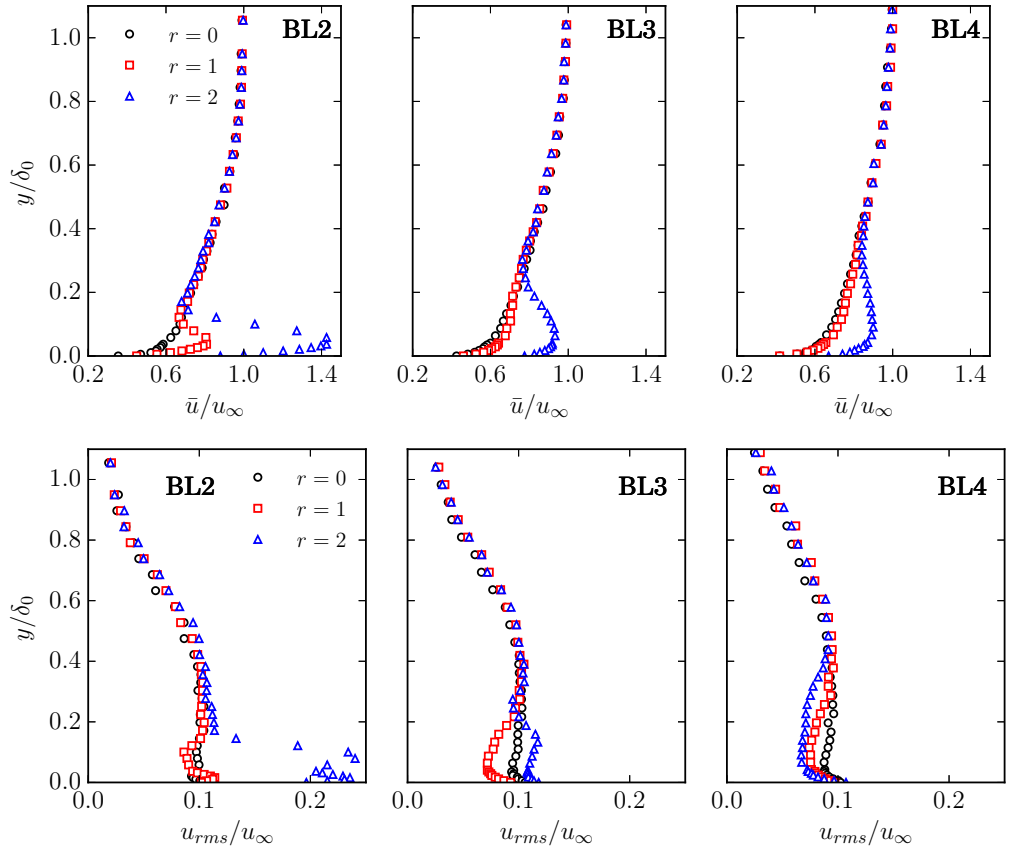

FIG. 8. Mean and root mean square velocity profiles for nozzle spacing $s = 2.5D$ at locations BL2, BL3 and BL4, corresponding to $x/D = 4, 14$ and 30, respectively.

cannot be clearly identified at increasing downstream locations with respect to SP2. As the individual jets merge, they form a smooth layer of low energy containing fluid below $y < 0.2\delta_0$ over the entire range of span length (z/D), see Fig. 6(c,d,g,h) and Fig. 7(c,d,g,h). At $r = 1$, the merging was observed in the vicinity of ST3 ($x/D = 14$), while at $r = 2$, the jets were observed to merge between ST3 ($x/D = 14$) and ST4 ($x/D = 30$). Although not reported for brevity, an increase in the spanwise spacing of the jet nozzles has been observed to result in a delay in the merging of the jets. Overall, it is important to underline that these multiple jets injections have the effect of reducing the energy content within the boundary layer, as observed in Fig. 6 and Fig. 7.

In order to investigate the streamwise evolution of the jets in crossflow along the wall-normal direction, and to examine the effects of the jets on the turbulent boundary layer, the streamwise velocity was measured over the entire boundary layer, at different streamwise locations downstream of the jet nozzles. The mean and *rms* velocity results are presented

r	σ	δ	θ			δ^*			u_τ		
		[mm]	[mm]			[mm]			[m/s]		
		(mean)	BL2	BL3	BL4	BL2	BL3	BL4	BL2	BL3	BL4
0	0	34	3.76	3.80	3.82	5.25	5.28	5.20	0.64	0.64	0.65
1	0.33	35	3.49	3.81	3.92	4.90	5.21	5.02	0.77	0.61	0.61
2	0.66	35	1.58	3.20	2.77	2.72	3.78	3.15	1.01	0.78	0.67

TABLE II. Boundary layer properties measured for the different jet velocity ratio cases at locations BL2, BL3 and BL4.

for $r = 0, 1$, and 2 in Fig. 8, at BL2, BL3 and BL4, corresponding to $x/D = 4, 14$ and 30, respectively. The baseline boundary layer ($r = 0$) is a canonical turbulent boundary layer, as confirmed by mean and *rms* velocity profiles (see Fig. 8), and by additional flow parameters such as the shape factor and skin friction coefficient that are not presented here for brevity. From the velocity profiles presented in Fig. 8, we can observe that the jets have a localized effect on the boundary layer downstream of the jet nozzles. The effects of the jets are confined to the lower third of the boundary layer at every location under analysis, and the velocity in the upper half of the boundary layer remains unaffected by the flow control method. The potential core of the jets remains close to the wall even at $x/D = 30$, which results in an increase in $\bar{u}$ below $0.3\delta_0$. Consistent with these observations, the boundary layer thickness (δ) is unaffected by the jets, and integral flow parameters such as the boundary layer displacement (δ^*) and the momentum thickness (θ) decrease, as presented in Table II. Additionally, the friction velocity (u_τ) grows due to the increased momentum near the wall. Moreover, from the observation of the mean velocity profiles in Fig. 8, the jets injections do not result in boundary layer separation, which seems to suggest that the aerodynamic behaviour of the flat plate is not significantly altered.

After understanding the flow pattern in proximity of the jet nozzles (Figs. 4 and 5), the effect of the jets on the energy content of the boundary layer can be assessed using the *rms* velocity results in Fig. 8. A reduction in the energy content of the flow structures is observed at BL3 for the lower velocity ratio ($r = 1$), while a higher energy content is measured for the higher velocity ratio at the same location. At BL4, a reduction in the energy content is observed at both blowing rates. The flow injection with higher velocity ratio results in a more

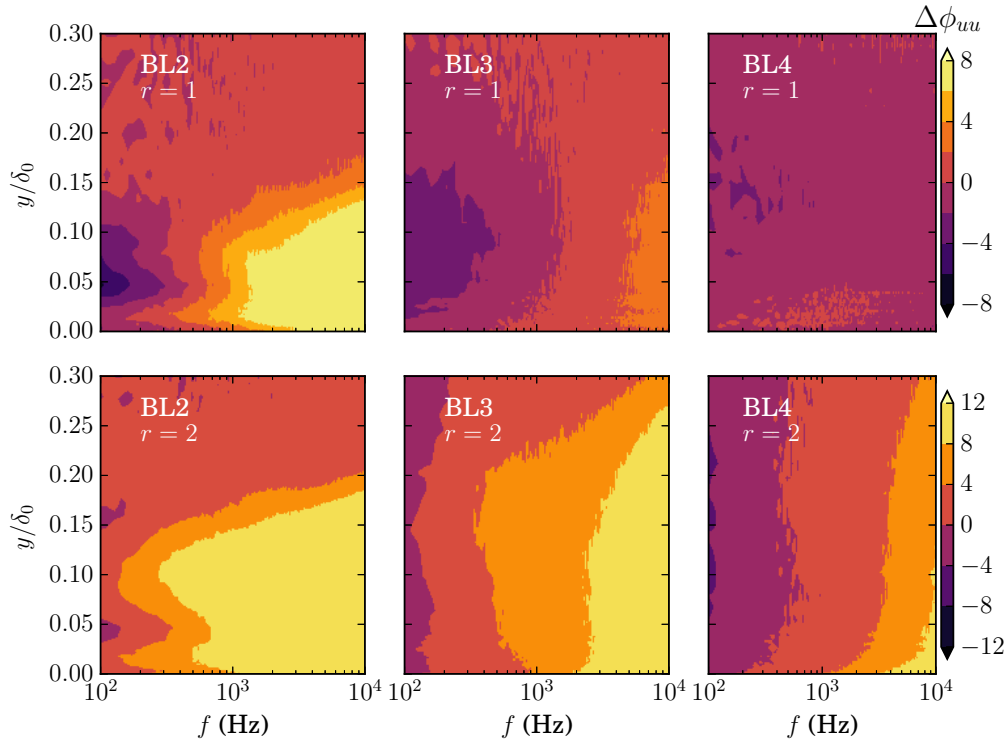

FIG. 9. Changes in the velocity power spectral density at BL2, BL3 and BL4 for velocity ratios $r = 1$ and $r = 2$ and for nozzle spacing $s = 2.5D$.

significant energy reduction at BL4 than $r = 1$. This reduction is significant both in terms of the magnitude and the wall-normal distance extent, and therefore it can be considered a robust effect of the jets injection on the boundary layer flow. It can be concluded that the multiple jets produce an initial increase in the flow energy content below $y = 0.2\delta_0$ at BL2 ($x/D = 4$), which drops below the baseline value farther downstream. The downstream location where this energy reduction occurs depends on the velocity ratio, r. The effect of the jets on the surface pressure fluctuations will be examined in Section III B.

The power spectral density (PSD) of the velocity fluctuations (ϕ_{uu}, dB/Hz) enables us to examine and quantify the changes in the turbulent energy content as a function of frequency. Figure 9 presents the change that the active flow control method causes on the velocity PSD ($\Delta\phi_{uu} = \phi_{uu,r\neq0} - \phi_{uu,r=0}$) in comparison with the baseline case, at locations BL2, BL3 and BL4. Analysing these PSD differences enables us to determine which turbulent motions lose energy as a consequence of jets injections into the boundary layer. Firstly, the lower velocity ratio ($r = 1$) is considered. From $\Delta\phi_{uu}$ results at BL2, the effect of the jets on the

flow is represented by the low energy content in the vicinity of $0.05\delta_0$, at low frequencies ($f < 600$ Hz). This evidences a reduction in the energy content of the larger turbulent structures. Reduction observed in the area of $y < 0.15\delta_0$ at $f < 600$ Hz also confirms, similarly to the u_{rms} results, that the jets produce a reduction in the energy content in the near-wall region. On the other hand, turbulent structures within the top shear layer of the jet ($y \approx 0.075\delta_0$), as seen in Figs. 5 and 8, causes an increase in the energy content of the flow at high frequencies. At BL2, a significant increase in the high frequency region ($f > 500$ Hz) can be observed at $y < 0.15\delta_0$, which diminishes downstream. It is worth stressing that the energy content of the velocity fluctuations is reduced over the whole frequency domain at the trailing-edge, as seen in the BL4 results. Concerning the higher jet velocity ratio ($r = 2$), similar observations can be made with respect to the spectra at BL2 and BL3. At BL4, an important reduction in the energy content is observed at lower frequencies ($f < 1$ kHz), while an increase of the spectral content occurs at frequencies $f > 1$ kHz.

B. The Effects of Jets Injection on the Surface Pressure Fluctuations

After showing how the jets alter the boundary layer and the energy content in the near-wall region, the surface pressure fluctuations are examined in this section. The root mean square of the surface pressure fluctuations (p_{rms}) was calculated from the pressure signals acquired at every flush mounted microphone location (see Fig. 1), which gives an indication of the footprint of the turbulent boundary layer on the wall. In this analysis of the pressure fluctuations, two parameters were varied, the jet spacing (s) and the velocity ratio (r). In particular, Fig. 10 shows the results of the *rms* pressure for a range of velocity ratios between $r = 1$ and $r = 2$, and for six different jet nozzle spacings ($s = 1.5D, 2.0D, 2.5D, 3.0D, 3.5D$ and $4.0D$). The root mean squares of the pressure fluctuations are presented at different downstream locations. The markers between BL3 and BL4 identify the downstream position where the minimum of each curve is located. In the analysis, p_{rms} is non-dimensionalised by the dynamic pressure of the free-stream flow, $p_\infty = \varrho u_\infty^2/2$, and it is presented along the streamwise direction (x/D). Results have shown that the trend of p_{rms} does not change significantly with the velocity ratio. The initial part of each curve has a negative slope, followed by an absolute minimum, and in the final stage, near the trailing-edge, p_{rms} exhibits a mild increase. The observed trend can be related to both the mean velocity and the energy

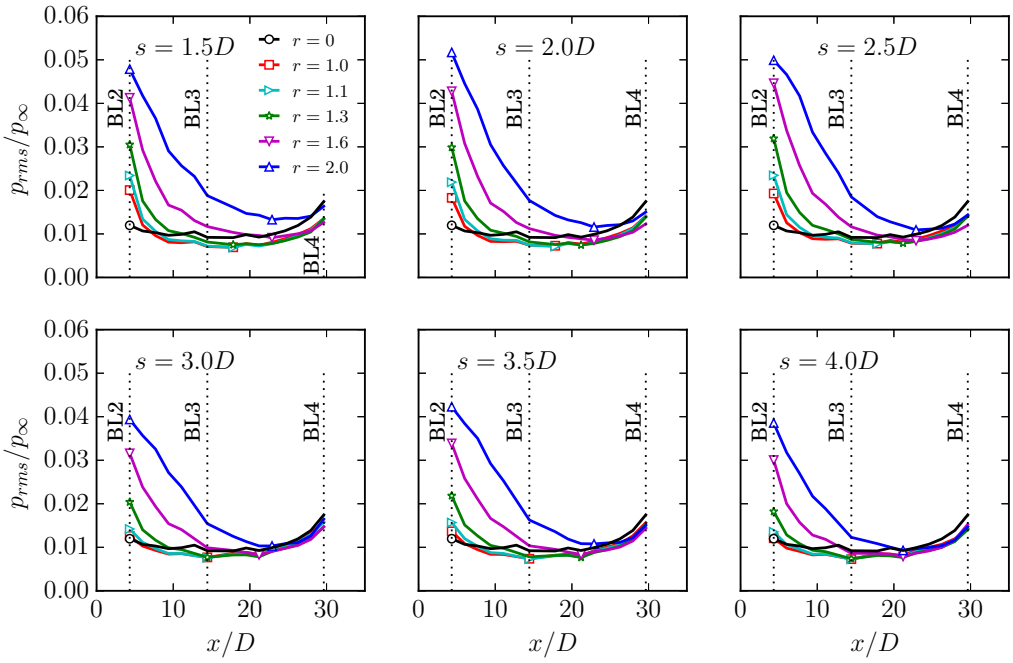

FIG. 10. Root mean square of surface pressure fluctuations measured in the streamwise direction for jet nozzle spacing configurations of $s = 1.5D, 2.0D, 2.5D, 3.0D, 3.5D$ and $4.0D$ and for varying velocity ratios r. The markers on each curve between BL3 and BL4 identify the locations where each of the p_{rms} curves reaches its minimum.

content results discussed in Section III A. Immediately downstream of the flow injection area, the jets are completely separated from each other, with no significant interaction. A significant increase in p_{rms} can be observed in this region. As seen in Figs. 6 and 7, the jets merge between BL3 and BL4 depending on the applied velocity ratio (r), and a stable layer of jet fluid develops. This stable layer is characterised by a low energy content. Once the minimum in p_{rms} is reached, flow recovery begins, which is indicated by the positive gradient in the curves past their respective minima. It is important to mention that the p_{rms} minima in Fig. 10 are observed at slightly different x locations for different velocity ratios (see markers between BL3 and BL4), as both r and s affect the development of the flow pattern. From the comparison between Fig. 7 and Fig. 10, we can notice that the minima in p_{rms} occur at the merging location of the jets. The observed trend of p_{rms} curves is also consistent with the u_{rms} profiles presented in Figs. 5 and 8. In Fig. 8 in particular, it can be seen that at BL3 the injection at $r = 1$ produces much lower values of u_{rms} than

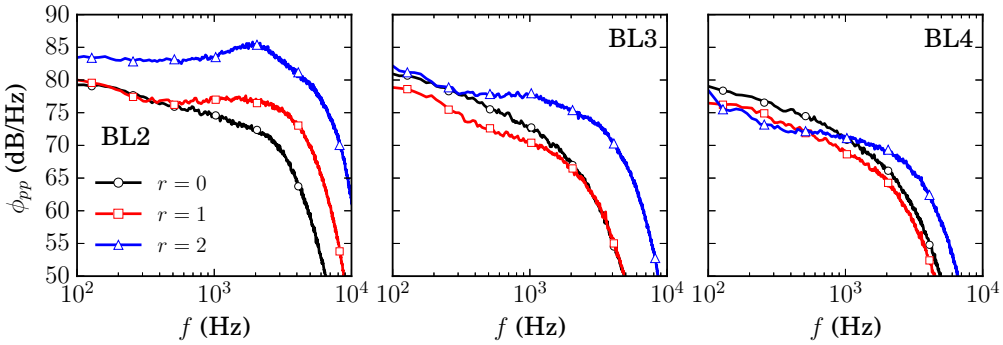

FIG. 11. Pressure power spectral density at BL2, BL3 and BL4 and for varying velocity ratios r and for nozzle spacing $s = 2.5D$.

at $r = 2$. Farther downstream, however, namely at BL4, the opposite phenomenon can be observed, and lower values of u_{rms} are this time obtained for a velocity ratio of $r = 2$. This is because the minimum in the downstream evolution of both u_{rms} and p_{rms} tends to move downstream at increasing velocity ratio r.

The necessary energy input to make the proposed flow control method work can be reduced by increasing the jet spacing, i.e. reducing the amount of air supplied to the system. However, increasing the distance between the jets (s) results in a mild increase of the minimum p_{rms}. In the majority of the gas turbine blade cooling studies (see Section I) a jet spacing of $s = 3.5D$ is applied to achieve a stable layer of jet fluid on the turbine blades. Nonetheless, as mentioned in Section I, the Reynolds number associated with the trailing-edge noise generation is significantly higher than in the case of the gas turbine blade cooling applications. Therefore, the high turbulence levels associated with aeroacoustic applications require a finer spacing of the jets to achieve significant reductions in p_{rms}. Additionally, in order to maximize the effects of the jets on the trailing-edge noise mitigation, the location of flow control should be chosen such that p_{rms} minimum occurs near the trailing-edge.

The surface pressure fluctuations play an important role in the far-field noise scattered by the trailing-edge. The behaviour of p_{rms} reveals the ideal streamwise location of the jet nozzles in order to maximize the favourable effects of the jets at the trailing-edge. The power spectral density of the pressure fluctuations (ϕ_{pp}) enables us to determine the frequency ranges over which the surface pressure fluctuations are reduced or increased as an effect of jets injection. The surface pressure PSD can be linked to the behaviour of the turbulence

intensity formerly seen in Figs. 5 and 8. In Fig. 11, the surface pressure power spectra are presented for BL2, BL3 and BL4, for velocity ratios of $r = 0, 1$ and 2. The results for the $r = 1$ injection case will be discussed first. At location BL2, an increase in ϕ_{pp} is observed for frequencies $f > 500$ Hz. This range overlaps with the region of increased energy content observed in $\Delta\phi_{uu}$ at BL2 (see Fig. 9). At BL3, where the jet flows are expected to merge together, a surface pressure PSD reduction of up to 5 dB is observed at low frequencies ($f < 1200$ Hz). Further downstream at BL4, results show that the use of the $r = 1$ injection leads to a robust reduction of the surface pressure PSD over the entire frequency range of interest. The PSD results presented in Fig. 11 are consistent with the p_{rms} results in Fig. 10 and the boundary layer energy content results in Figs. 8 and 9.

In the case of $r = 2$ jets injection, the boundary layer manipulation results in a significant increase in ϕ_{pp} at both the BL2 and BL3 locations, which is consistent with the observations from the u_{rms} and $\Delta\phi_{uu}$ presented in Figs. 8 and 9. The broadband hump observed at BL2 between 1 kHz and 3 kHz is examined later in this paper when discussing the pressure-velocity cross-spectra. The pressure fluctuations at BL4 for $f > 1$ kHz carry a larger spectral content than the baseline case, which is consistent with $\Delta\phi_{uu}$ at the same location (see Section III A). From ϕ_{pp}, it can be seen that the higher velocity ratio is more effective in reducing the pressure fluctuations in the low frequency region ($f < 1$ kHz) than the lower velocity ratio, at BL4. However, as shown in Fig. 11, the use of high-speed jets injection can lead to noise increase at high frequencies.

As shown in Figs. 9 and 11, the application of the inclined transverse jets alters the spectral content of both pressure and velocity fluctuations. In order to examine the spectral content of the velocity-pressure interaction, the coherence (normalized cross-spectra, γ^2_{pu}) was calculated between the surface pressure and velocity signals at different wall-normal locations. From a physical point of view, the velocity-pressure coherence (γ^2_{pu}) represents the frequency dependent relation between the turbulent flow structures and the surface pressure fluctuations. Therefore, this quantity establishes a link between the turbulence within the boundary layer and the surface pressure fluctuations exerted on the surface of the plate.

The pressure-velocity coherence is presented for the baseline case ($r = 0$) in Fig. 12(b), which provides an understanding on the contribution of the velocity fluctuations within the boundary layer to the surface pressure fluctuations. In order to identify the contribution

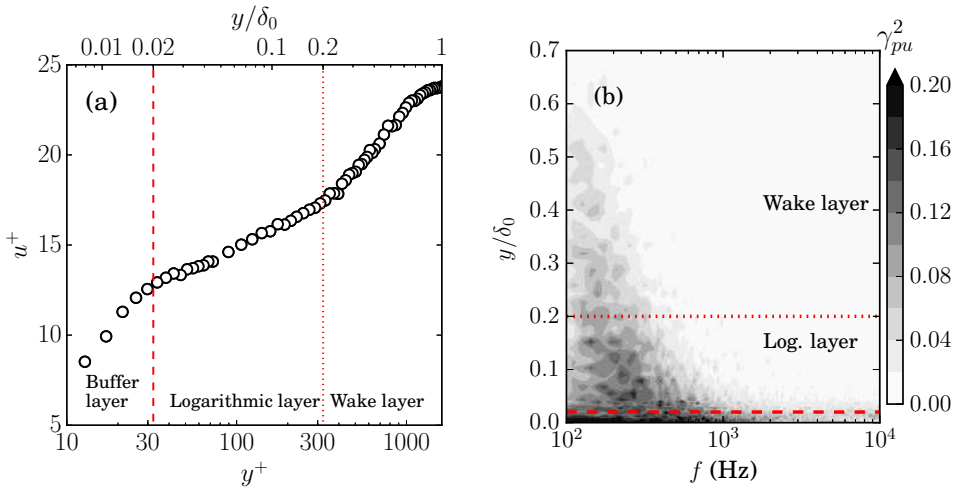

FIG. 12. Dimensionless velocity profile (a) and velocity-pressure cross-spectra (b) at BL4 ($x/D = 30$) of the turbulent boundary layer for the baseline case ($r = 0$) with the wall normal extent of the buffer layer, logarithmic layer and the wake layer also indicated in the figure.

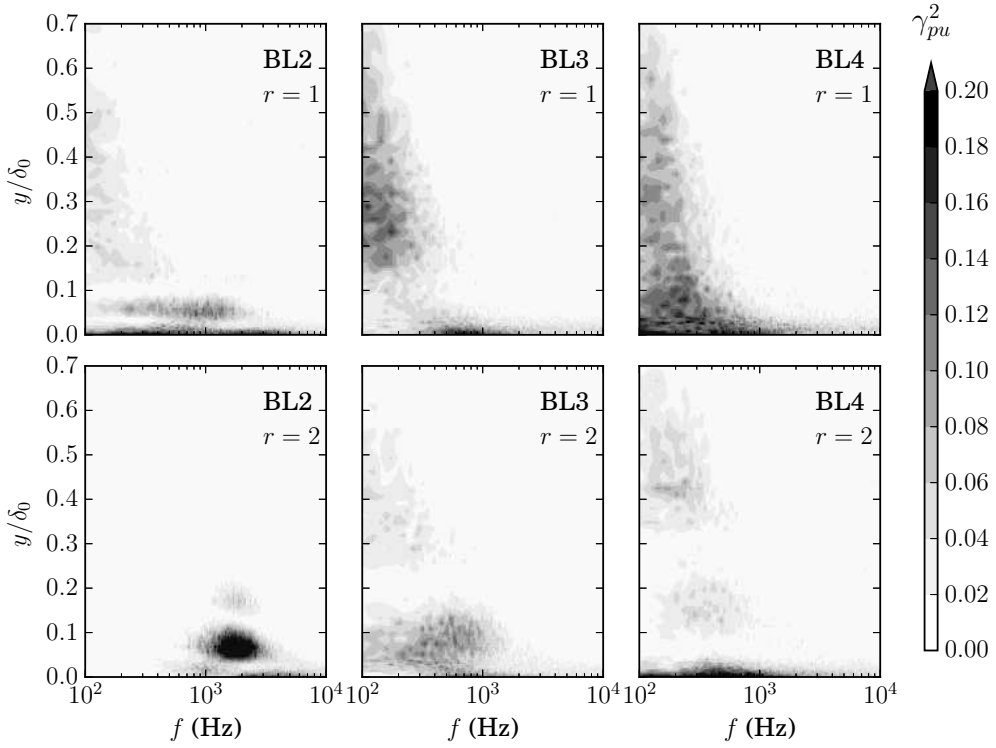

FIG. 13. Velocity-pressure cross-spectra at BL2, BL3 and BL4 for velocity ratios $r = 1$ and $r = 2$ and for nozzle spacing $s = 2.5D$.

of the different layers to ϕ_{pp}, Fig. 12(a) presents the limits of the buffer, logarithmic and wake layers for the baseline boundary layer ($r = 0$). As can be seen from Fig. 12(a), a portion of the buffer layer is resolved below $y^+ < 30$ ($y/\delta_0 < 0.02$). The logarithmic layer is located between $30 < y^+ < 300$ ($0.02 < y/\delta_0 < 0.2$), followed by the wake layer $300 < y^+ < 2000$ ($0.2 < y/\delta_0 < 1$) until the mean velocity reaches the value of the free-stream velocity. The boundary layer regions shown in Fig. 12(a) are in good agreement with the numerical data provided by Schlatter and Örlü[46] at a similar range of Reynolds number. In general, Fig. 12(b) reveals that the nearer the turbulent structures are to the wall, the more significant effect they play on the surface pressure fluctuations exerted on the surface. A significant amount of the contribution to ϕ_{pp} is originated from the velocity fluctuations below the logarithmic layer ($y < 0.02\delta_0$) over the entire range of investigated frequencies, see Fig. 12. The logarithmic layer ($y \approx 0.02 - 0.2\delta_0$) also plays a significant role in γ^2_{pu} at low frequencies ($f < 1$ kHz). Finally, the wake layer ($y > 0.2\delta_0$), where larger structures are located, is associated with lower levels of coherence at low frequencies.

Figure 13 shows the changes caused to the $p-u$ coherence map as a result of flow injection into the boundary layer at different jet velocity ratios. In the case of jets injection into the boundary layer, the flow undergoes significant changes, particularly in the near wall region ($y < 0.3\delta_0$), making the presentation of the data with respect to the boundary layer regions rather difficult. Therefore, in the following discussions on the effects of the jets injection ($r > 0$), the changes in γ^2_{pu} are analysed with respect to the baseline boundary layer regions. Firstly, the coherence obtained from the application of the lower velocity ratio ($r = 1$) is discussed. The results at BL2 indicate that the buffer layer ($y < 0.02\delta_0$) gives the highest contribution in terms of the velocity-pressure fluctuations. This reveals that the spectral increase formerly observed in both ϕ_{pp} and $\Delta\phi_{uu}$ at high frequencies originates from the lowest portion of the boundary layer. Another area of high correlation is found at BL2 ($x/D = 4$), at $y = 0.05\delta_0$, which is bounded both from the above and below by quiet areas of communication, i.e. low γ^2_{pu}. Concerning the location BL3 ($x/D = 14$), a region of low correlation is found at around $0.1\delta_0$, which separates the buffer layer and the wake layer. At BL3, the range of frequency where a low coherence was observed overlaps very well with the ranges characterised by a reduction in both ϕ_{pp} and ϕ_{uu}. From this, the flow control treatment seems to have the effect of cutting the communication between some coherent boundary layer structures with the surface, especially in the lower region of the boundary

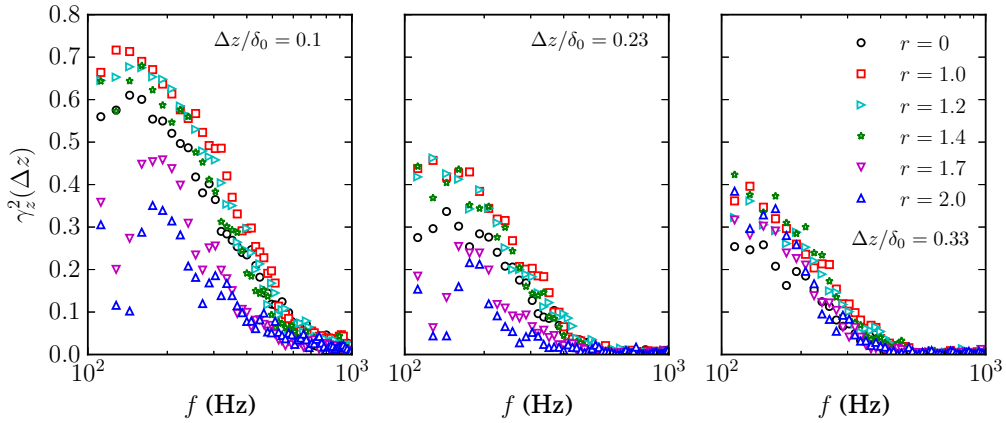

FIG. 14. Normalized cross-spectra (coherence) of spanwise microphone signals at $x/D = 27$ for a nozzle spacing of $s = 2.5D$.

layer ($y < 0.2\delta_0$). This mechanism contributes to the reduction of the surface pressure fluctuations. Considering the results obtained at BL4 ($x/D = 30$), the coherence builds up in the logarithmic layer ($0.02 < y < 0.2$), and γ^2_{pu} becomes similar to the baseline case, see Fig. 12. This indicates that the flow recovery begins at an earlier stage than BL4, which is in agreement with the p_{rms} results presented in Fig. 10.

Similar observations can be made regarding the γ^2_{pu} results for $r = 2$. At location BL2, a highly correlated area can be observed at the location of the jet potential core, i.e. within $y = 0.05 - 0.1\delta_0$, between 1 kHz and 3 kHz. This island of high correlation reveals that the cores of the multiple jets are responsible for the hump observed in the ϕ_{pp} results over the same frequency range (see Fig. 11). Similar to the results for the $r = 1$ case, the communication between the velocity and the pressure fluctuations is low in the areas adjacent to the jet core at BL2. Unlike the $r = 1$ case, these quiet areas of communication can still be observed at around $0.1\delta_0$ and $0.3\delta_0$ at BL4. It can therefore be concluded that jets injections at higher flow rates can lead to the suppression of the velocity-pressure coherence and emergence of quiet zone within the boundary layer over a longer streamwise distance. Finally, the coherence results presented in Fig. 13 reveal that the increase in ϕ_{pp} observed at high frequencies at BL4 is related to the near-wall small-scale structures, as the γ^2_{pu} results indicate an area of high correlation at BL4 within $0 < y/\delta_0 < 0.05$.

According to Amiet's model (see Section II C), the product of the spanwise extent of the turbulent length scales (Λ_z) and the surface pressure spectra (ϕ_{pp}) drives the generation of

far-field trailing-edge noise. While the pressure spectra is presented in Fig 11, an estimate of Λ_z is missing. In order to understand how the inclined jets affect the far-field noise, their effect on the spanwise extent of the turbulent structures is investigated in the following. Amiet defined the spanwise length scale of turbulent structures as shown in Eq. (3), where Λ_z is an integral quantity of the spanwise coherence, γ_z^2, over varying separation distances Δz. In order to examine the coherence at different Δz, microphone signals acquired at three spanwise spacings are considered, namely at $\Delta z/\delta_0 = 0.1, 0.23$ and 0.33, collected from the spanwise pressure transducer array located at $x/D = 27$, near the trailing-edge. An estimation of the spanwise extent of the turbulent structures within the flow (Λ_z) is presented in Fig. 15. This estimation was obtained from Eq. (3) using the trapezoidal integration scheme to integrate the spanwise coherence (γ_z^2). The spanwise coherence was calculated from surface pressure signals using five different microphone spacings, i.e. $\Delta z/\delta_0 = 0, 0.1, 0.13, 0.23$ and 0.33. It was found that the effect of transverse jets on the spanwise coherence, and therefore on the spanwise extent of the turbulent structures, is similar for all jet nozzle spacings. Therefore only the results related to $s = 2.5D$ are presented for brevity. The values of γ_z^2 and Λ_z (see Figs. 14 and 15) show that the injection of jets can lead to both an increase or a reduction of the spanwise extent of the turbulent length scales, depending on the jet velocity ratio. For $r < 1.7$, both γ_z^2 and Λ_z increase at all the frequencies under analysis, suggesting that the multiple jets increase the spanwise extent of the turbulent structures. For the jets operating at higher velocity ratios, $r \geq 1.7$, a significant broadband reduction of γ_z^2 is observed for $\Delta z/\delta_0 = 0.1$ and 0.23, while the spanwise coherence slightly increases for $\Delta z/\delta_0 = 0.33$. However, Fig. 15 reveals that jets injection with $r \geq 1.7$ can reduce the spanwise length of turbulent structures over all frequencies.

Figure 16 presents the far-field noise (S_{pp}) estimated using Amiets trailing-edge noise model[7] for an observer location being 1 m above the trailing-edge. As discussed in Section II C, the generation of the trailing-edge noise is driven by the product of the boundary layer quantities ϕ_{pp} and Λ_z, and therefore a reduction of the product of these two terms can result in the attenuation of the far-field trailing-edge noise. The far-field noise results show that the use of jets injection with a velocity ratio of $r = 1$ can result in the mild reduction of the trailing-edge noise over the whole frequency range under analysis. Increasing the jets injection rate to $r = 1.4$ leads to a much stronger far-field noise reduction, particularly at low frequencies. This is consistent with the surface pressure data observed in Fig. 11, and

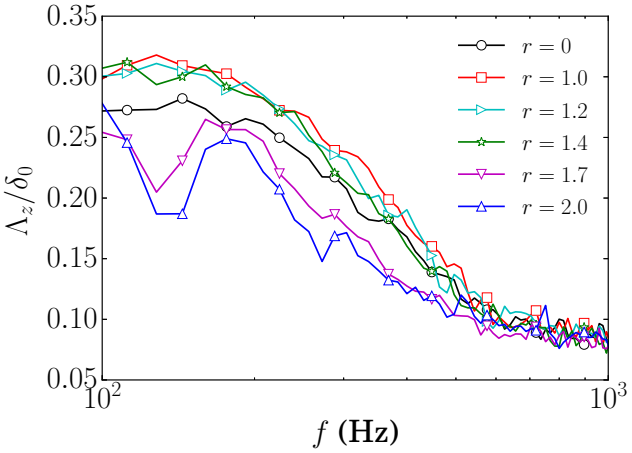

FIG. 15. Estimation of spanwise extent of turbulent structures at $x/D = 27$ for a nozzle spacing of $s = 2.5D$.

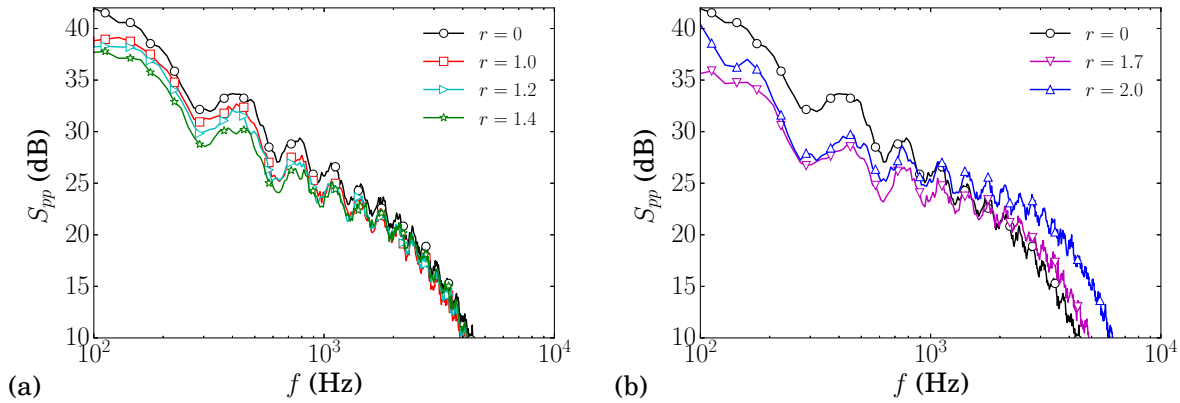

FIG. 16. Estimation of far-field noise for jet velocity ratios (a) $r < 1.7$ and (b) $r \geq 1.7$ using Amiet's trailing edge noise model with the observer located at a vertical distance of 1 m above the trailing edge.

also shows that the increase in the spanwise extent of the turbulent structures observed at low frequencies in Fig. 15 does not affect the noise reduction performances of the jets at low injection rates. At higher injection rates ($r \geq 1.7$), the far-field noise data show that a strong reduction of trailing-edge noise, of up to 5 dB, can be achieved at low frequencies ($f < 1 - 2$ kHz). However, as seen in Fig. 16, the use of high speed jets can also lead to an increase of radiated noise at high frequencies, which is again consistent with the surface

pressure results in Fig. 11. To summarize, the estimates of far-field noise show that the use of both the low speed and high-speed jets can reduce the far-field noise, and can be used in various engineering applications, such as engine or propeller airfoils or wind turbine blades.

IV. CONCLUSIONS

The current work investigates a flow control method for the reduction of trailing-edge noise. An array of inclined transverse jet nozzles with a uniform spanwise distribution is installed on a flat plate rig upstream of a trailing-edge, with the aim of controlling the hydrodynamic pressure field associated with the turbulent boundary layer. Simultaneous measurement of velocity with the use of hot-wire anemometry, and surface pressure fluctuations using flush mounted microphones is performed at a number of locations downstream of the active flow control treatment. Results are collected at different jet velocity ratios (r), which is the ratio of jet velocity to free-stream velocity. The developing flow pattern was measured for a low ($r = 1$) and a high ($r = 2$) jet velocity ratio case. A wide range of jet spacings were also considered.

The turbulence statistics reveal that the interaction between the jets and the boundary layer generates a stable fluid layer characterised by a low energy content. The jet flow associated with low energy content resulted in the reduction of the surface pressure fluctuation energy exerted on the surface beneath the boundary layer. According to Amiet's model of trailing-edge noise, the product between the power spectra of surface pressure fluctuations (ϕ_{pp}) and the spanwise extent of turbulent length scales (Λ_z) is proportional to the far-field noise scattered from the trailing-edge. The pressure-velocity cross-spectral studies revealed that the fluid layer associated with low energy content decouples the communication between the velocity fluctuations and surface pressure fluctuations, which contributes to the attenuation of the power spectra of surface pressure fluctuations (ϕ_{pp}). In particular, the application of jets with lower velocity ratios ($r < 1.7$) resulted in a broadband reduction of ϕ_{pp} at the trailing-edge, while at higher velocity ratios ($r \geq 1.7$) the reduction was more significant at low frequencies with a slight noise penalty at high frequencies. The spanwise extent of the turbulent length scales is also affected by the application of the inclined jets. Jets introduced to the boundary layer with a low velocity ratio ($r < 1.7$) resulted in a slight increase of the spanwise extent of turbulent structures (Λ_z). When feeding the

jets into the boundary layer with a higher velocity ratio ($r \geq 1.7$), they were capable of significantly reducing the spanwise extent of turbulent structures (Λ_z). The estimation of far-field trailing-edge noise using Amiet's model revealed that transverse jets at low velocity ratios ($r < 1.7$) result in a broadband reduction of the radiated noise. At high velocity ratios ($r \geq 1.7$), a reduction of far-field noise at low frequencies up to 5 dB was obtained, even if the far-field noise was found to increase at high frequencies. Future developments of the present work will involve the measurement of far-field noise to better understand the underlying phenomena responsible for the reduction of trailing-edge noise.

REFERENCES

[1]T. F. Brooks and T. H. Hodgson, "Trailing edge noise prediction from measured surface pressures," Journal of Sound and Vibration **78**, pp. 69–117 (1981).

[2]T. F. Brooks, D. S. Pope, and M. A. Marcolini, "Airfoil self-noise and prediction," NASA Technical Report (1989).

[3]J. E. F. Williams and D. L. Hawkings, "Sound generation by turbulence and surfaces in arbitrary motion," Philosopical Transactions of the Royal Society London **264**, pp. 321–342 (1969).

[4]J. E. Ffowcs-Williams and L. H. Hall, "Aerodynamic sound generation by turbulent flow and in the vicinity of a scattering half plane," Journal of Fluid Mechanics **40**, pp. 657–670 (1970).

[5]R. K. Amiet, "Acoustic radiation from an airfoil in a turbulent stream," Journal of Sound and Vibration **41**, 407 – 420 (1975).

[6]D. M. Chase, "Noise radiated from an edge in turbulent flow," AIAA Journal **13**, 1041–1047 (1975).

[7]R. K. Amiet, "Noise due to turbulent flow past a trailing edge," Journal of Sound and Vibration **47(3)**, 387–393 (1976).

[8]International Civil Aviation Organization, "Aircraft noise to the convention on international civil aviation," Volume I., Annex 16. (1971).

[9]T. Chong, A. Vathylakis, P. Joseph, and M. Gruber, "Self-Noise Produced by an Airfoil with Nonflat Plate Trailing-Edge Serrations," AIAA Journal **51**, 2665–2677 (2013).

[10]B. Lyu, M. Azarpeyvand, and S. Sinayoko, "Prediction of noise from serrated trailing

edges," Journal of Fluid Mechanics **793**, 556–588 (2016).

[11]S. L. Prigent, O. R. H. Buxton, and P. J. K. Bruce, "Coherent structures shed by multiscale cut-in trailing edge serrations on lifting wings," Physics of Fluids **29**, 075107 (2017).

[12]M. Herr and W. Dobrzynski, "Experimental investigations in low-noise trailing-edge design," AIAA Journal **43**, 1167–1175 (2005).

[13]T. Geyer, E. Sarradj, and C. Fritzsche, "Measurement of the noise generation at the trailing edge of porous airfoils," Experiments in Fluids **48**, 291–308 (2010).

[14]S. Showkat Ali, M. Szőke, and M. Azarpeyvand, "Trailing edge bluntness flow and noise control using porous treatments," in *22nd AIAA/CEAS Aeroacoustics Conference*, AIAA-2016-2832 (2016).

[15]A. Afshari, M. Azarpeyvand, A. A. Dehghan, and M. Szőke, "Trailing edge noise reduction using novel surface treatments," in *22nd AIAA/CEAS Aeroacoustics Conference*, AIAA-2016-2834 (2016).

[16]A. Afshari, M. Azarpeyvand, A. A. Dehghan, and M. Szőke, "Three-dimensional surface treatments for trailing edge noise reduction," in *23rd International Congress on Sound & Vibration, Athens, Greece* (2016).

[17]Q. Ai, M. Azarpeyvand, X. Lachenal, and P. M. Weaver, "Aerodynamic and aeroacoustic performance of airfoils with morphing structures," Wind Energy **19**, 1325–1339 (2016), we.1900.

[18]H. K. Jawahar, Q. Ai, and M. Azarpeyvand, "Experimental and numerical investigation of aerodynamic performance for airfoils with morphed trailing edges," Renewable Energy **127**, 355–367 (2018).

[19]A. Wolf, T. Lutz, W. Würz, E. Krämer, O. Stalnov, and A. Seifert, "Trailing edge noise reduction of wind turbine blades by active flow control," Wind Energy **18**, 909–923 (2014).

[20]S. Moreau, P. Laffay, A. Idier, and N. Atalla, "Several noise controls of the trailing-edge noise of a controlled-diffusion airfoil," in *22nd AIAA/CEAS Aeroacoustics Conference*, AIAA-2016-2816 (2016).

[21]D. Matera, *Validation of the noise prediction code Rnoise and reduction of trailing edge noise by active flow control*, Ph.D. thesis, Università Degli Studi Di Padova (2013).

[22]T. Lutz, B. Arnold, A. Wolf, and E. Krämer, "Numerical studies on a rotor with distributed suction for noise reduction," Journal of Physics: Conference Series **524**, 012122 (2014).

[23]M. Szőke and M. Azarpeyvand, "Active flow control methods for the reduction of trailing edge noise," in *23rd AIAA/CEAS Aeroacoustics Conference*, AIAA-2017-3004 (2017).

[24]M. Szőke, D. Fiscaletti, and M. Azarpeyvand, "The use of micro-jets for airfoil self-noise control," in *24th AIAA/CEAS Aeroacoustics Conference* (2018).

[25]R. J. Margason, "Fifty years of jet in cross flow research," in *In AGARD, Computational and Experimental Assessment of Jets in Cross Flow 41 p (SEE N94-28003 07-34)* (1993).

[26]K. Mahesh, "The interaction of jets with crossflow," Annual Review of Fluid Mechanics **45**, 379–407 (2013).

[27]D. G. Hyams and J. H. Leylek, "A detailed analysis of film cooling physics: part III - streamwise injection with shaped holes," in *International Gas Turbine and Aeroengine Congress and Exhibition* (ASME, 1997).

[28]I. V. Iourokina and S. K. Lele, "Large eddy simulation of film-cooling above the flat surface with a large plenum and short exit holes," in *44th Aerospace Sciences Meeting and Exhibit, Reno, NV*, AIAA-2006-1102 (2006).

[29]A. Rozati and D. K. Tafti, "Large-eddy simulations of leading edge film cooling: Analysis of flow structures, effectiveness, and heat transfer coefficient," International Journal of Heat and Fluid Flow **29**, 1–17 (2008).

[30]D. K. Walters and J. H. Leylek, "A detailed analysis of film–cooling physics: Part i - streamwise injection with cylindrical holes," in *International Gas Turbine and Aeroengine Congress and Exhibition* (ASME, 1997).

[31]P. Taylor, "An investigation of a jet exhausting from a plate at incidence into a crosswind," Vertica **1**, 307–315 (1977).

[32]P. Taylor and D. J. Watkins, "An investigation of inclined jets in a crosswind," AGARD-CP-308 (1981).

[33]K. Aoyagi and P. K. Snyder, "Experimental investigation of a jet inclined to a subsonic crossflow," in *AIAA and NASA Ames VSTOL Conference, Palo Alto, CA, U.S.A.*, AIAA-2610 (1981).

[34]S. Gopalan, B. M. Abraham, and J. Katz, "The structure of a jet in cross flow at low velocity ratios," Physics of Fluids **16**, 2067–2087 (2004).

[35]S. J. Kline and F. A. McClintock, "Describing uncertainties in single-sample experiments," Mechanical Engineering **75**, 3–8 (1953).

[36]G. Schewe, "On the structure and resolution of wall-pressure fluctuations associated with

turbulent boundary-layer flow," Journal of Fluid Mechanics **134**, 311–328 (1983).

[37]G. M. Corcos, "Resolution of pressure in turbulence," The Journal of the Acoustical Society of America **35**, 192–199 (1963).

[38]R. M. Gray and J. W. Goodman, *Fourier transforms: an introduction for engineers*, Vol. 322 (Springer Science & Business Media, 2012).

[39]R. A. Antonia, Y. Zhu, and M. Sokolov, "Effect of concentrated wall suction on a turbulent boundary layer," Physics of Fluids **7**, 2465–2474 (1995).

[40]R. R. Parchen, "Progress report draw: A prediction scheme for trailing edge noise based on detailed boundary layer characteristics," TNO Report (1998).

[41]M. Roger and S. Moreau, "Broadband self-noise from loaded fan blades," AIAA Journal **42** (2004).

[42]R. Kelso and A. Smits, "Horseshoe vortex systems resulting from the interaction between a laminar boundary layer and a transverse jet," Physics of Fluids **7**, 153–158 (1995).

[43]A. R. Karagozian, "The jet in crossflow," Physics of Fluids **26**, 1–47 (2014).

[44]J. Pietrzyk, D. Bogard, and M. Crawford, "Hydrodynamic measurements of jets in crossflow for gas turbine film cooling applications," ASME J. Turbomach **111**, 139–145 (1989).

[45]R. Sau and K. Mahesh, "Dynamics and mixing of vortex rings in crossflow," Journal of Fluid Mechanics **604**, 389–409 (2008).

[46]P. Schlatter and R. Örlü, "Assessment of direct numerical simulation data of turbulent boundary layers," Journal of Fluid Mechanics **659**, 116–126 (2010).